Langmuir
Article
pubs.acs.org/Langmuir

Self-Cleaning Diffractive Macroporous Films by Doctor Blade Coating

Hongta Yang and Peng Jiang*

Department of Chemical Engineering, University of Florida, Gainesville, Florida 32611

Received May 27, 2010. Revised Manuscript Received June 28, 2010

Here we report a scalable bottom-up technology for creating three-dimensionally highly ordered macroporous polymer films with excellent water-repelling and optical diffractive properties. A simple doctor blade coating process is first utilized to create silica colloidal crystal−polymer nanocomposites. The close-packed silica spheres are selectively removed to fabricate flexible macroporous polymer films with crystalline arrays of voids which are interconnected through small nanopores. The size of the voids can be easily controlled by tuning the duration of an oxygen reactive-ion etching process prior to the removal of the templating silica spheres. After surface functionalization with fluorosilane, superhydrophobic surface with large apparent water contact angle and small sliding angle can be obtained. The water-repelling property can be quantitatively explained by adapting the Cassie's dewetting model. We further demonstrate that self-cleaning functionality can be achieved on superhydrophobic macroporous coatings by preventing bacterial contamination. The high crystalline quality of the macroporous polymers also enables strong optical diffraction from the periodic lattice. The optical properties are evaluated by normal-incidence reflectance measurements and theoretical calculation using a scalar-wave approximation model. A good agreement between theory and experiment has been obtained. The simultaneous achievement of controlled dewetting and strong optical diffraction by templated porous films could open new applications in self-cleaning diffractive optics.

Introduction

Inspired by the unique water-repelling property of lotus leaves, superhydrophobic coatings with large water contact angle ($>150°$) and small sliding angle ($<10°$) have attracted great recent interests.[1−5] These biomimetic coatings are of considerable technological importance in developing self-cleaning surfaces,[6] antifouling substrates,[6] antifogging coatings,[7,8] efficient microfluidic devices,[9,10] bioseparation media,[11] anticorrosive coatings,[12,13] and more. A large variety of technologies, such as layer-by-layer (LBL) assembly,[7,14−16] lithography,[17−20] phase separation,[21,22] electrospinning,[23−25] plasma etching,[9,26] and electrochemical treatment,[27,28] have been developed to create superhydrophobic coatings. As air is the most hydrophobic material, porous coatings with a large fraction of entrapped air have been widely exploited to control the wettability of the films. Various methodologies, like LBL assembly of nanoparticles and polyelectrolytes,[7,16] breath figure-based assembly,[29,30] block copolymer microphase separation,[31,32] glancing angle deposition,[33] sol−gel processing,[34−38]

*To whom correspondence should be addressed. E-mail: pjiang@che.ufl.edu.

(1) Li, X. M.; Reinhoudt, D.; Crego-Calama, M. *Chem. Soc. Rev.* **2007**, *36*, 1350–1368.
(2) Liu, M. J.; Zheng, Y. M.; Zhai, J.; Jiang, L. *Acc. Chem. Res.* **2010**, *43*, 368–377.
(3) Ma, M. L.; Hill, R. M. *Curr. Opin. Colloid Interface Sci.* **2006**, *11*, 193–202.
(4) Roach, P.; Shirtcliffe, N. J.; Newton, M. I. *Soft Matter* **2008**, *4*, 224–240.
(5) Zhang, X.; Shi, F.; Niu, J.; Jiang, Y. G.; Wang, Z. Q. *J. Mater. Chem.* **2008**, *18*, 621–633.
(6) Genzer, J.; Efimenko, K. *Biofouling* **2006**, *22*, 339–360.
(7) Cebeci, F. C.; Wu, Z. Z.; Zhai, L.; Cohen, R. E.; Rubner, M. F. *Langmuir* **2006**, *22*, 2856–2862.
(8) Gao, X. F.; Yan, X.; Yao, X.; Xu, L.; Zhang, K.; Zhang, J. H.; Yang, B.; Jiang, L. *Adv. Mater.* **2007**, *19*, 2213–2217.
(9) Tsougeni, K.; Papageorgiou, D.; Tserepi, A.; Gogolides, E. *Lab Chip* **2010**, *10*, 462–469.
(10) Boreyko, J. B.; Chen, C. H. *Phys. Rev. Lett.* **2009**, *103*, 174502.
(11) Han, Y. H.; Levkin, P.; Abarientos, I.; Liu, H. W.; Svec, F.; Frechet, J. M. J. *Anal. Chem.* **2010**, *82*, 2520–2528.
(12) Barkhudarov, P. M.; Shah, P. B.; Watkins, E. B.; Doshi, D. A.; Brinker, C. J.; Majewski, J. *Corros. Sci.* **2008**, *50*, 897–902.
(13) Xu, Q. F.; Wang, J. N. *New J. Chem.* **2009**, *33*, 734–738.
(14) Choi, W.; Tuteja, A.; Mabry, J. M.; Cohen, R. E.; McKinley, G. H. *J. Colloid Interface Sci.* **2009**, *339*, 208–216.
(15) Ma, M. L.; Gupta, M.; Li, Z.; Zhai, L.; Gleason, K. K.; Cohen, R. E.; Rubner, M. F.; Rutledge, G. C. *Adv. Mater.* **2007**, *19*, 255–259.
(16) Zhai, L.; Cebeci, F. C.; Cohen, R. E.; Rubner, M. F. *Nano Lett.* **2004**, *4*, 1349–1353.
(17) Oner, D.; McCarthy, T. J. *Langmuir* **2000**, *16*, 7777–7782.
(18) Krupenkin, T. N.; Taylor, J. A.; Schneider, T. M.; Yang, S. *Langmuir* **2004**, *20*, 3824–3827.
(19) Furstner, R.; Barthlott, W.; Neinhuis, C.; Walzel, P. *Langmuir* **2005**, *21*, 956–961.
(20) Krupenkin, T. N.; Taylor, J. A.; Wang, E. N.; Kolodner, P.; Hodes, M.; Salamon, T. R. *Langmuir* **2007**, *23*, 9128–9133.
(21) Xie, Q. D.; Fan, G. Q.; Zhao, N.; Guo, X. L.; Xu, J.; Dong, J. Y.; Zhang, L. Y.; Zhang, Y. J.; Han, C. C. *Adv. Mater.* **2004**, *16*, 1830–1835.
(22) Zhao, N.; Xie, Q. D.; Weng, L. H.; Wang, S. Q.; Zhang, X. Y.; Xu, J. *Macromolecules* **2005**, *38*, 8996–8999.
(23) Han, D. W.; Steckl, A. J. *Langmuir* **2009**, *25*, 9454–9462.
(24) Wu, H.; Zhang, R.; Sun, Y.; Lin, D. D.; Sun, Z. Q.; Pan, W.; Downs, P. *Soft Matter* **2008**, *4*, 2429–2433.
(25) Zhan, N. Q.; Li, Y. X.; Zhang, C. Q.; Song, Y.; Wang, H. G.; Sun, L.; Yang, Q. B.; Hong, X. *J. Colloid Interface Sci.* **2010**, *345*, 491–495.
(26) Park, S. G.; Moon, H. H.; Lee, S. K.; Shim, J.; Yang, S. M. *Langmuir* **2010**, *26*, 1468–1472.
(27) Yan, H.; Kurogi, K.; Mayama, H.; Tsujii, K. *Angew. Chem., Int. Ed.* **2005**, *44*, 3453–3456.
(28) Zhang, X.; Shi, F.; Yu, X.; Liu, H.; Fu, Y.; Wang, Z. Q.; Jiang, L.; Li, X. Y. *J. Am. Chem. Soc.* **2004**, *126*, 3064–3065.
(29) Yabu, H.; Shimomura, M. *Chem. Mater.* **2005**, *17*, 5231–5234.
(30) Yabu, H.; Takebayashi, M.; Tanaka, M.; Shimomura, M. *Langmuir* **2005**, *21*, 3235–3237.
(31) Levkin, P. A.; Svec, F.; Frechet, J. M. J. *Adv. Funct. Mater.* **2009**, *19*, 1993–1998.
(32) Tung, P. H.; Kuo, S. W.; Jeong, K. U.; Cheng, S. Z. D.; Huang, C. F.; Chang, F. C. *Macromol. Rapid Commun.* **2007**, *28*, 271–275.
(33) Tsoi, S. F.; Fok, E.; Sit, J. C.; Veinot, J. G. C. *Chem. Mater.* **2006**, *18*, 5260–5266.
(34) Erbil, H. Y.; Demirel, A. L.; Avci, Y.; Mert, O. *Science* **2003**, *299*, 1377–1380.
(35) Han, J. T.; Lee, D. H.; Ryu, C. Y.; Cho, K. W. *J. Am. Chem. Soc.* **2004**, *126*, 4796–4797.
(36) Bhagat, S. D.; Oh, C. S.; Kim, Y. H.; Ahn, Y. S.; Yeo, J. G. *Microporous Mesoporous Mater.* **2007**, *100*, 350–355.
(37) Latthe, S. S.; Imai, H.; Ganesan, V.; Rao, A. V. *Microporous Mesoporous Mater.* **2010**, *130*, 115–121.
(38) Shirtcliffe, N. J.; McHale, G.; Newton, M. I.; Perry, C. C.; Roach, P. *Mater. Chem. Phys.* **2007**, *103*, 112–117.

template-assisted nanofabrication,[39−45] and electron irradiation of nanocomposites,[42,46] have been demonstrated to produce superhydrophobic porous coatings.

Spontaneous crystallization of colloidal particles is a simple, fast, and inexpensive approach for creating water-repellent coatings.[47−58] The self-assembled colloidal arrays can also be used as template to create superhydrophobic macroporous films.[59−62] These macroporous films with crystalline arrays of voids are intrinsic photonic crystals and are of great technological importance in developing diffractive optical devices for all-optical integrated circuits.[63,64] Polymeric macroporous membranes with interconnecting voids have also been demonstrated as separation media for macromolecules and DNA[65,66] and biosensors.[67] Unfortunately, most of the current colloidal self-assembly and templating technologies are not compatible with standard industrial fabrication and only favorable for low volume, laboratory-scale production. It is highly desirable to develop a roll-to-roll compatible bottom-up technology for large-scale production of multifunctional macroporous coatings with unique self-cleaning, optical, and size-exclusive separation functionalities.

We have recently developed a roll-to-roll compatible doctor blade coating (DBC) technology for creating three-dimensional highly ordered colloidal crystal−polymer nanocomposites and self-standing macroporous polymer membranes.[68] In DBC, an immobilized doctor blade applies a unidirectional shear force to align particles in a colloidal suspension that passes through a small gap between the blade and a moving substrate.[69] We have demonstrated that the templated macroporous membranes with interconnecting voids and uniform nanopores can be directly used as filtration membranes to achieve size exclusive separation of particles.[68] Here we show that multifunctional macroporous coatings with unique combination of self-cleaning and optical diffractive properties can be fabricated by a simple bottom-up technology. The very top layer of the porous coating entraps a large fraction of air and thus enables a superhydrophobic surface, while the internal ordered multilayers creates strong optical diffraction. These self-assembled porous films could find important technological applications in self-cleaning diffractive optical devices.

Experimental Section

Materials and Substrates. The reagents used for silica particle synthesis including tetraethyl orthosilicate (TEOS) (98%) and ammonium hydroxide (NH_4OH) (28%) are purchased from Sigma-Aldrich. Ethanol (200 proof) is obtained from Pharmaco Products. Ethoxylated trimethylolpropane triacrylate monomer (ETPTA, SR 454) and photoinitiator, Darocur 1173 (2-hydroxy-2-methyl-1-phenyl-1-propanone), are provided by Sartomer and Ciba-Geigy, respectively. (Tridecafluoro-1,1,2,2,-tetrahydrooctyl)trichlorosilane (97%) used for surface modification is purchased from Alfa Aesar. All solvents and chemicals are of reagent quality and are used without further purification except for TEOS, which is freshly distilled before use. The silicon wafer primer, 3-acryloxypropyltrichlorosilane (APTCS), is obtained from Gelest. Silicon wafers (4 in., test grade, n type, (100), Wafernet) are cleaned in a "piranha" solution (a 3:1 mixture of concentrated sulfuric acid with 30% hydrogen peroxide) for half an hour, rinsed with Milli-Q water (18.2 MΩ cm), and then dried in a stream of nitrogen. *Escherichia coli*−ampicillin (Sigma-Aldrich) is used as model bacterium for self-cleaning test. Luria−Bertani (LB) medium used for bacterial culture is purchased from Sigma-Aldrich.

Instrumentation. Scanning electron microscopy (SEM) is performed on a JEOL 6335F FEG-SEM. A thin layer of gold is sputtered onto the samples prior to imaging. The photopolymerization of ETPTA monomer is carried out on a pulsed UV curing system (RC 742, Xenon). A KD Scientific 780-230 syringe pump is used to precisely control the DB-coating speed. Oxygen reactive-ion etching (RIE) is performed on a Unaxis Shuttlelock RIE/ICP reactive-ion etcher. Normal incidence optical reflection spectra are obtained by using an Ocean Optics HR4000 high-resolution fiber-optic Vis−near-IR spectrometer with a reflection probe. The apparent water contact angle is measured by using a dynamic contact angle analyzer (Ramé-Hart goniometer) at ambient temperature with a droplet volume of 0.013 mL.

Preparation of Colloidal Suspensions. The synthesis of monodispersed silica microspheres with less than 5% diameter variation is performed by following the well-established Stöber method.[70] In a typical synthesis, 50 mL of freshly distilled TEOS is rapidly added to a mixture of 650 mL of 200-proof ethanol, 55.7 mL of deionized water, and 23.1 mL of 28% aqueous ammonia. The solution is stirred at ambient temperature for 8 h. The as-synthesized silica particles are purified in 200-proof ethanol by five centrifugation−ultrasonication cycles to remove impurities, such as ammonia, water, and unreacted TEOS. The purified silica microspheres are centrifuged and redispersed in ETPTA monomer (with 1 wt % Darocur 1173 as photoinitiator) using a Thermolyne vortex mixer. The final particle volume fraction of

(39) Aulin, C.; Yun, S. H.; Wagberg, L.; Lindstrom, T. *ACS Appl. Mater. Interface* **2009**, *1*, 2443–2452.
(40) Cao, L. L.; Price, T. P.; Weiss, M.; Gao, D. *Langmuir* **2008**, *24*, 1640–1643.
(41) Lai, Y. K.; Huang, Y. X.; Wang, H.; Huang, J. Y.; Chen, Z.; Lin, C. J. *Colloids Surf., B* **2010**, *76*, 117–122.
(42) Lee, E. J.; Kim, J. J.; Cho, S. O. *Langmuir* **2010**, *26*, 3024–3030.
(43) Ran, C. B.; Ding, G. Q.; Liu, W. C.; Deng, Y.; Hou, W. T. *Langmuir* **2008**, *24*, 9952–9955.
(44) Zhu, S. J.; Li, Y. F.; Zhang, J. H.; Lu, C. L.; Dai, X.; Jia, F.; Gao, H. N.; Yang, B. *J. Colloid Interface Sci.* **2010**, *344*, 541–546.
(45) Li, Y.; Duan, G. T.; Cai, W. P. *J. Colloid Interface Sci.* **2007**, *314*, 615–620.
(46) Lee, E. J.; Lee, H. M.; Li, Y.; Hong, L. Y.; Kim, D. P.; Cho, S. O. *Macromol. Rapid Commun.* **2007**, *28*, 246–251.
(47) Shiu, J. Y.; Kuo, C. W.; Chen, P. L.; Mou, C. Y. *Chem. Mater.* **2004**, *16*, 561–564.
(48) Zhang, L.; Zhou, Z. L.; Cheng, B.; DeSimone, J. M.; Samulski, E. T. *Langmuir* **2006**, *22*, 8576–8580.
(49) Wang, J. X.; Hu, J. P.; Wen, Y. Q.; Song, Y. L.; Jiang, L. *Chem. Mater.* **2006**, *18*, 4984–4986.
(50) Tsai, H. J.; Lee, Y. L. *Langmuir* **2007**, *23*, 12687–12692.
(51) Xiu, Y. H.; Zhu, L. B.; Hess, D. W.; Wong, C. P. *Langmuir* **2006**, *22*, 9676–9681.
(52) Zhao, Y.; Li, M.; Lu, Q. H.; Shi, Z. Y. *Langmuir* **2008**, *24*, 12651–12657.
(53) Zhang, G.; Wang, D. Y.; Gu, Z. Z.; Mohwald, H. *Langmuir* **2005**, *21*, 9143–9148.
(54) Ming, W.; Wu, D.; van Benthem, R.; de With, G. *Nano Lett.* **2005**, *5*, 2298–2301.
(55) Brozell, A. M.; Muha, M. A.; Abed-Amoli, A.; Bricarello, D.; Parikh, A. N. *Nano Lett.* **2007**, *7*, 3822–3826.
(56) Wang, J. X.; Wen, Y. Q.; Hu, J. P.; Song, Y. L.; Jiang, L. *Adv. Funct. Mater.* **2007**, *17*, 219–225.
(57) Kim, S. H.; Lee, S. Y.; Yang, S. M. *Angew. Chem., Int. Ed.* **2010**, *49*, 2535–2538.
(58) Min, W. L.; Jiang, B.; Jiang, P. *Adv. Mater.* **2008**, *20*, 3914–3918.
(59) Li, J.; Fu, J.; Cong, Y.; Wu, Y.; Xue, L. J.; Han, Y. C. *Appl. Surf. Sci.* **2006**, *252*, 2229–2234.
(60) Gu, Z. Z.; Uetsuka, H.; Takahashi, K.; Nakajima, R.; Onishi, H.; Fujishima, A.; Sato, O. *Angew. Chem., Int. Ed.* **2003**, *42*, 894–897.
(61) Li, H. L.; Wang, J. X.; Yang, L. M.; Song, Y. L. *Adv. Funct. Mater.* **2008**, *18*, 3258–3264.
(62) Sato, O.; Kubo, S.; Gu, Z. Z. *Acc. Chem. Res.* **2009**, *42*, 1–10.
(63) Blanco, A.; Chomski, E.; Grabtchak, S.; Ibisate, M.; John, S.; Leonard, S. W.; Lopez, C.; Meseguer, F.; Miguez, H.; Mondia, J. P.; Ozin, G. A.; Toader, O.; van Driel, H. M. *Nature* **2000**, *405*, 437–440.
(64) Vlasov, Y. A.; Bo, X. Z.; Sturm, J. C.; Norris, D. J. *Nature* **2001**, *414*, 289–293.
(65) Liu, L.; Li, P. S.; Asher, S. A. *Nature* **1999**, *397*, 141–144.
(66) Nykypanchuk, D.; Strey, H. H.; Hoagland, D. A. *Science* **2002**, *297*, 987–990.
(67) Qian, W. P.; Gu, Z. Z.; Fujishima, A.; Sato, O. *Langmuir* **2002**, *18*, 4526–4529.
(68) Yang, H.; Jiang, P. *Langmuir*, submitted.
(69) Mistler, R. E.; Twiname, E. R. *Tape Casting: Theory and Practice*; American Ceramic Society: Westerville, OH, 2000.
(70) Stober, W.; Fink, A.; Bohn, E. *J. Colloid Interface Sci.* **1968**, *26*, 62–69.

the colloidal suspensions is controlled to be 50%. After filtration through a 5 μm syringe filter (Whatman) to remove any large particle aggregates, the transparent and viscous solution is stored in an open vial in dark for overnight to allow residual ethanol to evaporate.

Doctor Blade Coating. A commercial doctor blade (Fisher, 4 cm wide) is placed vertically on the surface of a silicon wafer which has been freshly primed by APTCS. The silica−ETPTA suspension is dispensed along one sidewall of the blade onto the wafer. The wafer is then dragged in a controlled speed by a syringe pump to move the colloidal suspension across the gap between the doctor blade and the substrate.[68] The ETPTA momoner is finally photopolymerized by exposure to ultraviolet radiation using a pulsed UV curing system for 4 s.

Preparation of Macroporous Polymer Films. An oxygen reactive-ion etcher operated at 40 mTorr oxygen pressure, 40 sccm oxygen flow rate, and 100 W is used to partially remove ETPTA matrix for releasing the embedded silica particles. The templating silica spheres are selectively removed by dropping a 2 vol % hydrofluoric acid aqueous solution on the silica/ETPTA nanocomposite for 10 s, followed by washing in ethanol. These procedures are repeated for three times until the ETPTA film becomes transparent in ethanol.

Surface Modification of Macroporous Polymer Films. The hydrophobicity of macroporous ETPTA films can be improved by surface functionalization using fluorosilanes with low surface energy. The as-prepared macroporous ETPTA films are placed in a sealed vessel with a beaker containing a small amount of (tridecafluoro-1,1,2,2-tetrahydrooctyl)trichlorosilane. The vessel is then pumped to evaporate the fluorosilane to react with the moisture and the hydroxyl groups on the surface of macroporous ETPTA films.

Water Contact Angle Measurements. The apparent water contact angle is measured using a goniometer (NRL C.A. goniometer, Ramé-Hart Inc.) with autopipetting and imaging systems. Using the autopipetting system and DROPimage advanced software, a 13 μL water droplet is dispensed onto the sample surface. Apparent water contact angle is determined by using ImageJ v1.37 with the drop analysis plugin. Some manual adjustment of the 7-knot snake is required before the curve can be snaked accurately. Analysis of each image yields a left and right contact angle. This process is repeated eight times for each sample, yielding 16 angle measurements per sample. The average of these 16 values is the apparent contact angle reported.

Self-Cleaning Test. The self-cleaning properties of the templated macroporous polymer films are evaluated by measuring the bacterial contamination after the samples are exposed to *Escherichia coli*−ampicillin solution. During the experiment, samples with different wettability are cut into 2×2 cm^2 specimens and placed on a sterilized plastic substrate. 0.05 mL of *Escherichia coli*−ampicillin solution with 5×10^4 colony forming units (CFU) per milliliter is uniformly sprayed on the surface of the specimens. The specimens are then offered an inclining angle of 5° for 5 s right after the *Escherichia coli*−ampicillin solution is sprayed. The specimens are finally submerged in Luria−Bertani (LB) broth medium and cultured at 37 °C for 24 h before measuring the equivalent CFU. All experiments are performed in dark.

Normal Incidence Optical Reflection Measurements. An Ocean Optics spectrometer with a reflection probe is used for reflectance measurements. A calibrated halogen light source is used to illuminate the sample. The beam spot size is about 3 mm on the sample surface. Measurements are performed at normal incidence and the cone angle of collection is less than 5°. Absolute reflectivity is obtained as ratio of the sample spectrum and the reference spectrum. The reference spectrum is the optical density obtained from an aluminum-sputtered (1000 nm thickness) silicon wafer. Final value of absolute reflectivity is the average of several measurements obtained from different spots on the sample surface.

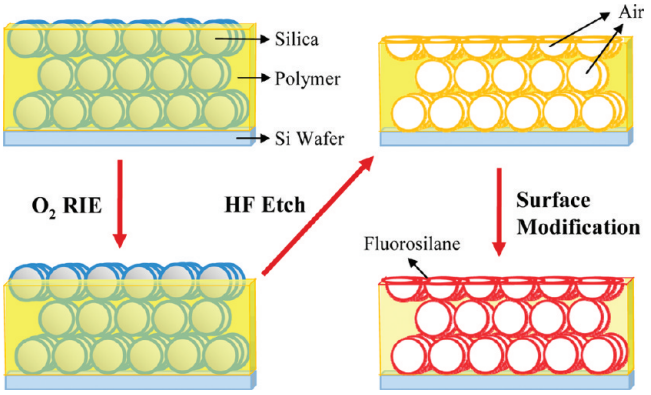

Figure 1. Schematic illustration of the experimental procedures for preparing superhydrophobic macroporous polymer films.

Results and Discussion

Figure 1 shows the schematic illustration of the experimental procedures for preparing multifunctional macroporous polymer films. We start to fabricate 3D highly ordered silica colloidal crystal−polymer nanocomposites by using a simple and scalable doctor blade coating technology.[68] In a typical DBC process, monodispersed silica microspheres with diameter ranging from 200 to 700 nm are dispersed in a nonvolatile monomer, ethoxylated trimethylolpropane triacrylate (ETPTA), to make colloidal suspensions with particle volume fraction of ca. 50%. An immobilized and vertically beveled razor blade which gently touches with a substrate applies a uniform shear force to align silica microspheres when the substrate is moved at a controlled speed. The monomer is finally photopolymerized to form colloidal crystal−polymer nanocomposites. The shear-aligned particles are close-packed and embedded in an ETPTA matrix. The protrusion depth of the top-layer silica spheres can be controlled by briefly applying oxygen reactive-ion etching (RIE) for various durations. The templating silica spheres can then be completely removed by etching in a 2 vol % hydrofluoric acid aqueous solution. The resulting macroporous polymer film is finally surface-modified by exposing to a vapor of (tridecafluoro-1,1,2,2-tetrahydrooctyl)trichlorosilane with low surface energy. This silane coupling agent can be readily hydrolyzed with the surface moisture on the macroporous polymer to form reactive silanolic hydroxyl groups that can condense with the hydroxyl groups on the surface of macroporous polymer created by oxygen RIE treatment.[71] Similar surface modification of polymers (e.g., PMMA) with fluorosilanes has been widely used in creating releasing promoter layers for nanoimprint lithography.[72]

Figure 2 shows top-view SEM images of macroporous ETPTA films templated from 260 nm silica spheres. These films are prepared by plasma etching a DB-coated nanocomposite at 40 mTorr oxygen pressure, 40 sccm oxygen flow rate, and 100 W for 5, 10, 20, 25, 30, and 40 s, followed by selective removal of the templating silica spheres. The size of the top-layer voids is measured by averaging over 100 cavities, and the results are summarized in Figure 3. From Figures 2 and 3, it is evident that the void size increases with the oxygen RIE time at the beginning. When the etching time reaches ~30 s, the top hemispheres of silica particles are exposed, resulting in the maximum void size (239 ± 13 nm) which is close to the diameter of templating silica spheres.

(71) Plueddemann, E. P. *Silane Coupling Agents*, 2nd ed.; Plenum Press: New York, 1991.
(72) Houle, F. A.; Rettner, C. T.; Miller, D. C.; Sooriyakumaran, R. *Appl. Phys. Lett.* **2007**, *90*, 213103.

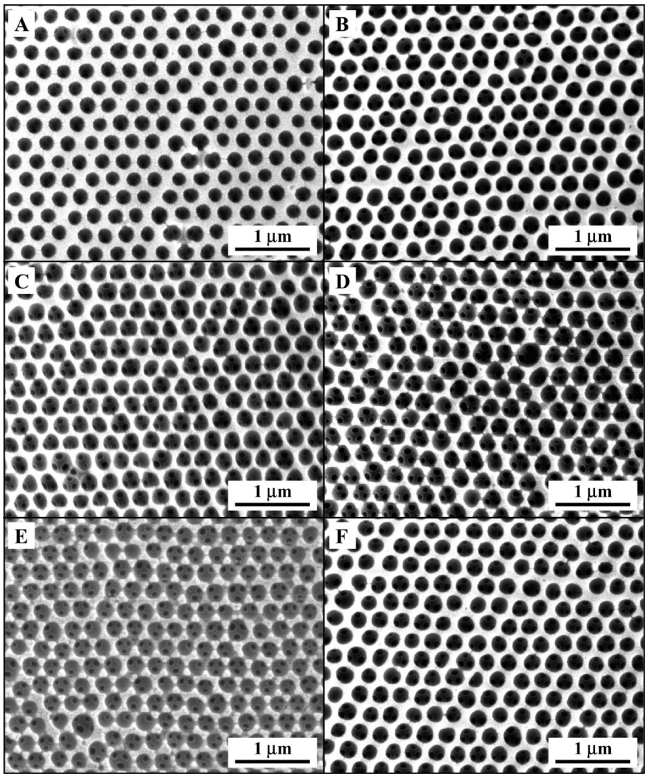

Figure 2. Top-view SEM images of macroporous ETPTA films templated from 260 nm silica spheres. These films were prepared by plasma etching a DB-coated nanocomposite at 40 mTorr oxygen pressure, 40 sccm oxygen flow rate, and 100 W for (A) 5, (B) 10, (C) 20, (D) 25, (E) 30, and (F) 40 s, followed by selective removal of the templating silica spheres.

After that, smaller voids are obtained as only the bottom parts of the silica spheres are templated. Another interesting feature of these macroporous polymer films is the small nanopores that interconnect the large voids defined by the silica spheres. These nanopores are originated from the touching sites between neighboring particles in the original colloidal crystal−polymer nanocomposites.[63,64,73] We have previously demonstrated that these uniform nanopores enable the size exclusive separation of particles with different sizes.[68]

The apparent water contact angles (CA) of the fluorosilane-modified macroporous ETPTA films are measured by a dynamic contact angle analyzer. Figure 4A−C shows the water drop profiles used to determine the apparent water CAs on macroporous ETPTA films after 0, 30, and 40 s oxygen RIE treatments. Figure 4D compares averaged apparent water CAs of macroporous ETPTA films etched at different RIE durations. It is apparent that the water CAs follow the same trend as the size of the voids with different etching durations as shown in Figure 3. A maximum water CA of 155 ± 1° is achieved at 30 s oxygen RIE time. This demonstrates that superhydrophobic surfaces can be obtained on the surface-modified macroporous polymer films, although the apparent water CAs of a flat ETPTA film (without oxygen RIE) and a fluorosilane-modified flat ETPTA film are only 78 ± 3° and 115 ± 1°, respectively.

The above static water CA alone is insufficient for the complete evaluation of the dewetting properties of the templated macroporous

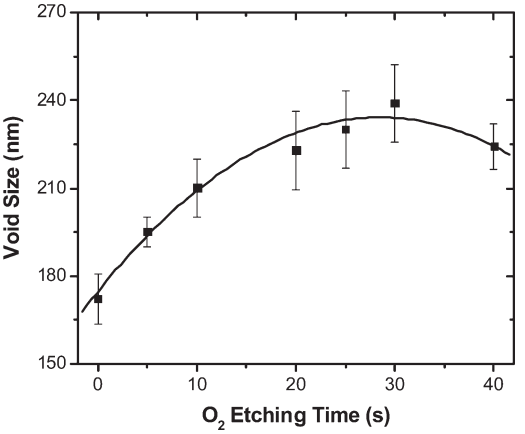

Figure 3. Dependence of the void size of macroporous ETPTA films templated from 260 nm silica spheres vs oxygen RIE etching time.

polymer films.[74] We therefore measure the advancing and receding contact angles associated with the increase and decrease of droplet volumes using the above dynamic contact angle analyzer. Panels A and B in Figure 5 show the water drop profiles used to measure the advancing and receding CAs on the superhydrophobic macroporous ETPTA film after 30 s oxygen RIE treatment. The corresponding advancing and receding CAs are 156° and 152°. The measured dynamic CAs and sliding angles for macroporous ETPTA films etched at different oxygen RIE durations are summarized in Figure 5C,D. Once again, we find a clear trend of the sliding angle with the size of the templated voids. The sliding angle becomes smaller when the void size increases. By comparing Figures 5D and 4D, it is evident that a larger apparent water CA is associated with a smaller sliding angle.

The experimental results on the wettability of macroporous polymer films can be quantitatively explained by adapting the traditional dewetting models.[75,76] In Wenzel's model,[76] complete wetting of all surface features (interconnecting voids in this case) leads to eq 1:

$$\cos\theta' = r\cos\theta \quad (1)$$

where θ' is the apparent CA on a rough surface, θ is the intrinsic CA on a flat surface, and r is the surface roughness factor defined by the ratio of the total area in contact with the liquid to the projected area. If Wenzel's wetting occurs, the filling of air cavities by water will lead to a higher efficient refractive index and a smaller refractive index contrast. This will cause a red shift of the Bragg diffraction peak and reduced reflection amplitude. However, the templated macroporous films retain the shining green color even after complete immersion in water. We therefore adapted Cassie's model to explain our experimental observations.[75] In Cassie wetting, the liquid droplet wets a composite surface consisting of both solid (polymer in this case) and entrapped air. This incomplete wetting can be described by the Cassie equation

$$\cos\theta' = f\cos\theta - (1-f) \quad (2)$$

where f is the fraction of the area of the polymer in direct contact with the liquid droplet.

(73) Velev, O. D.; Jede, T. A.; Lobo, R. F.; Lenhoff, A. M. *Nature* **1997**, *389*, 447–448.
(74) Miwa, M.; Nakajima, A.; Fujishima, A.; Hashimoto, K.; Watanabe, T. *Langmuir* **2000**, *16*, 5754–5760.
(75) Cassie, A. B. D.; Baxter, S. *Trans. Faraday Soc.* **1944**, *40*, 546–550.
(76) Wenzel, R. N. *Ind. Eng. Chem.* **1936**, *28*, 988–994.

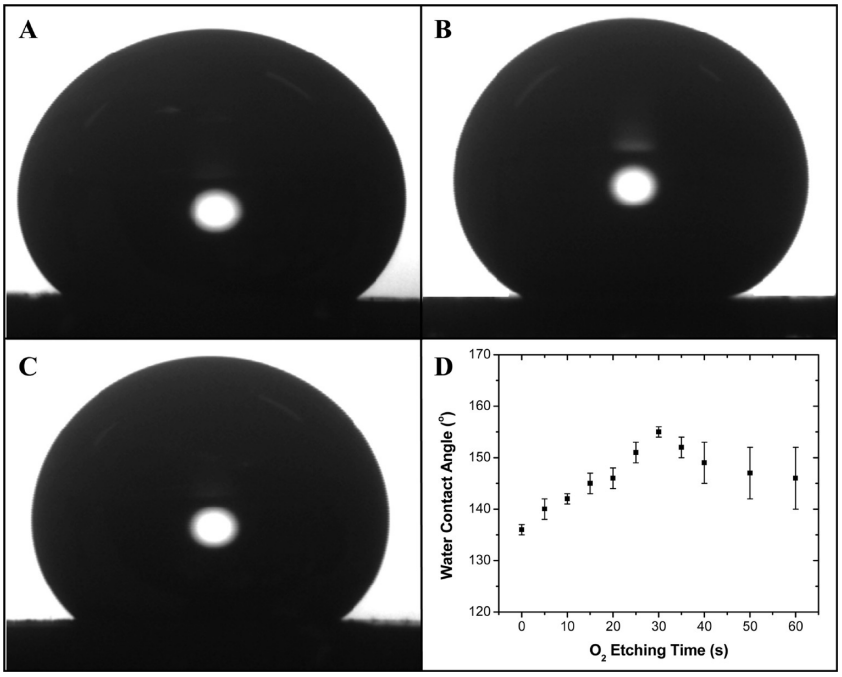

Figure 4. (A−C) Water drop profiles on fluorosilane-modified macroporous ETPTA films after 0, 30, and 40 s oxygen plasma etching. (D) Apparent water contact angles of fluorosilane-modified macroporous ETPTA films etched at different RIE durations.

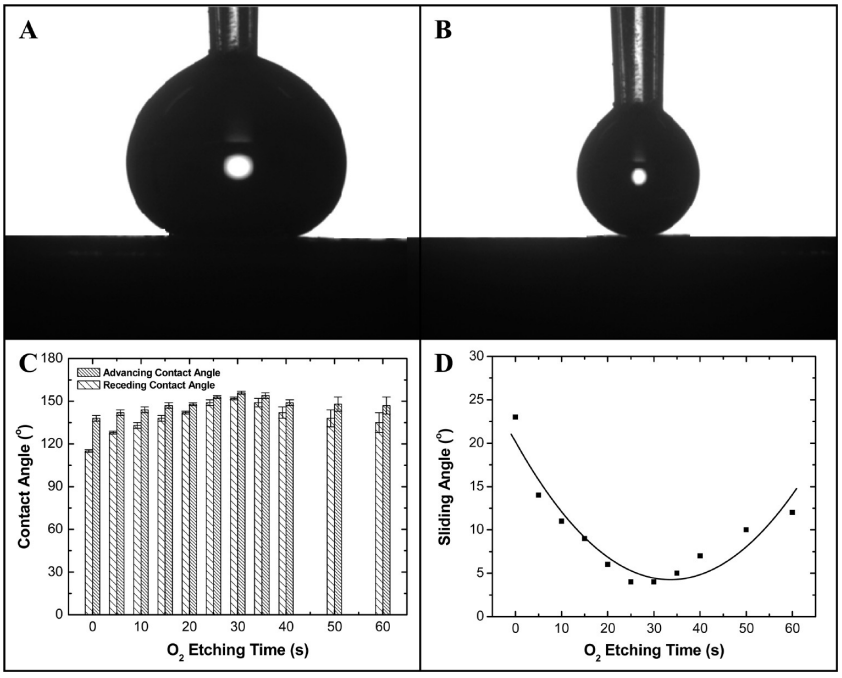

Figure 5. (A, B) Water drop profiles used to determine the advancing and receding water contact angles on a fluorosilane-modified macroporous ETPTA film after 30 s oxygen RIE. (C) Advancing and receding water contact angles of fluorosilane-modified macroporous ETPTA film etched at different RIE durations. (D) Sliding angles of fluorosilane-modified macroporous ETPTA film etched at different RIE durations.

We can estimate the area fraction of the polymer/water interface, f, by using a simple trigonometric calculation as

$$f = 1 - \frac{\pi {R_v}^2}{2\sqrt{3}{R_s}^2} \quad (3)$$

where R_v is the radius of voids measured by the top-view SEM images as shown in Figure 2 and R_s is the radius of the templating silica spheres. The calculated water CAs using the Cassie's model are compared with the experimental data in Figure 6. The slopes of the experimental and theoretical results are comparable, though the experimental CAs are slightly larger than the theoretical predictions. This is reasonable as we assume the water droplet forms a flat surface on the macroporous film to derive eq 3. In reality, the water droplet will slightly penetrate into the top-layer voids. This will increase the contact area of water and

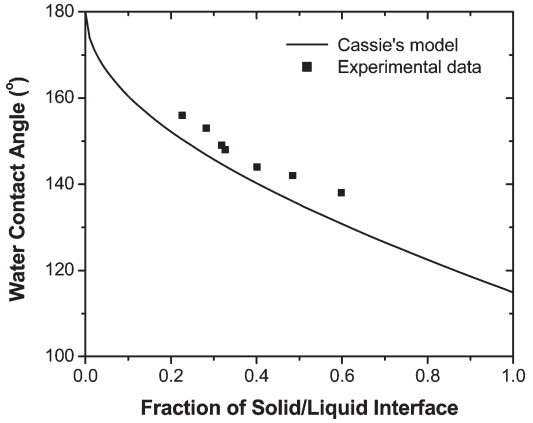

Figure 6. Dependence of the apparent water contact angle vs the fraction of solid/liquid (i.e., polymer/water) interface, f. The solid line is calculated using Cassie's equation.

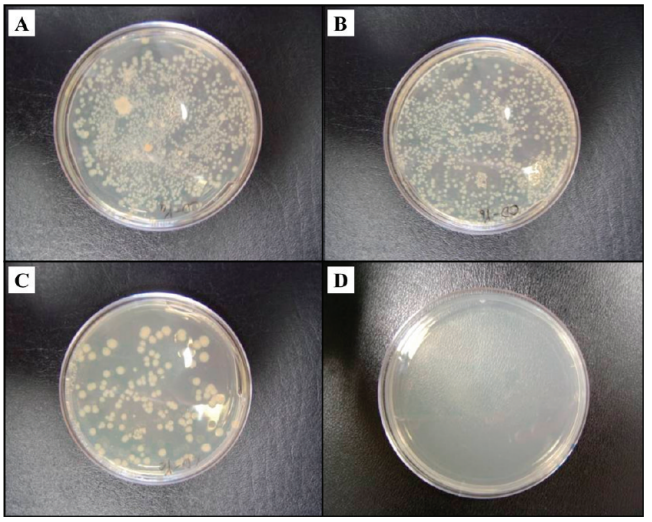

Figure 7. Bacterial cultures on four specimens after applying an inclining angle of 5° for 5 s: (A) flat ETPTA film; (B) fluorosilane-modified flat ETPTA film; (C) fluorosilane-modified macroporous ETPTA film without oxygen RIE; (D) fluorosilane-modified macroporous ETPTA film after 30 s oxygen RIE.

entrapped air and thus leads to a larger effective $(1-f)$, in other words, a smaller effective f. This will move the experimental data closer to the theoretically predicted curve. Further experiments show that macroporous ETPTA membranes templated from larger silica spheres (560 and 700 nm) exhibit similar dewetting behavior as depicted in Figure 6, indicating the Cassie's model is still valid for these large-pores films.

We have shown above that superhydrophobic surface with large CA (> 150°) and small sliding angle (< 5°) can be obtained on fluorosilane-modified macroporous polymer films. This unique combination is highly favorable for developing self-cleaning coatings.[19,77] We further evaluate the self-cleaning properties of the macroporous films by measuring the bacterial contamination after the samples are exposed to *Escherichia coli*−ampicillin solution. After spraying 0.05 mL of *Escherichia coli*−ampicillin solution with 5×10^4 CFU/mL on the surface of the samples, the specimens are inclined at an angle of 5° for 5 s. The specimens are finally submerged in Luria−Bertani broth medium and cultured

(77) Sun, T. L.; Feng, L.; Gao, X. F.; Jiang, L. *Acc. Chem. Res.* **2005**, *38*, 644–652.

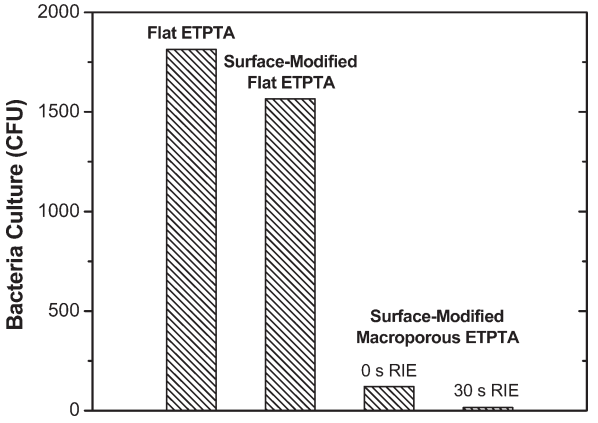

Figure 8. Counts of the colony forming units for the samples in Figure 7.

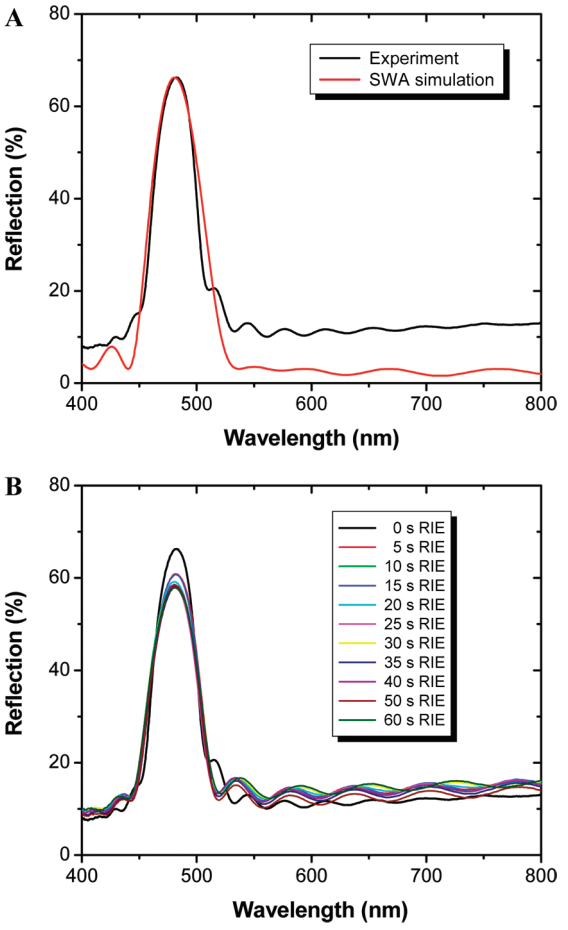

Figure 9. (A) Experimental (black line) and SWA-simulated (red line) optical reflection spectra at normal incidence from a macroporous ETPTA film with 260 nm air cavities and 12 layers. (B) Comparison of normal-incidence optical reflection spectra from macroporous ETPTA films etched at different RIE durations.

at 37 °C for 24 h before measuring the equivalent CFU. Figure 7 displays the photographs of bacterial cultures of *Escherichia coli*−ampicillin on a flat ETPTA film, a surface-modified flat ETPTA film, a surface-modified macroporous ETPTA film without oxygen RIE treatment, and a surface-modified macroporous ETPTA film with 30 s oxygen RIE. The counted colony forming units for these four samples are shown in Figure 8. Compared with a flat ETPTA specimen with a water CA of

78 ± 3°, ~86% of bacteria are left on the surface-modified flat ETPTA specimen (water CA of 115 ± 1°), nearly 8% of bacteria are left on the surface-modified macroporous ETPTA specimen without RIE treatment (water CA of 136 ± 1°), and less than 1% of bacteria are left on the surface-modified macroporous ETPTA specimen with the maximum water CA (155 ± 1°). The significant lowering of the bacterial contamination on the macroporous ETPTA specimen with small sliding angle is due to the fact that most of the bacterial solution rolls off from the superhydrophobic surface when an inclining angle of 5° is applied.

Besides the self-cleaning functionality facilitated by the superhydrophobic surface layer, the 3D highly ordered structure of the bulk macroporous polymer films could enable other important technological applications in diffractive optics (e.g., filters, optical switches, and low-threshold lasers).[78−80] We evaluate the optical properties and the crystalline quality of macroporous polymer films by measuring their optical reflectance at normal incidence using an Ocean Optics Vis−near-IR spectrometer with a reflection probe. The experimental reflectance spectrum in Figure 9A (dark line) shows distinctive peaks caused by Bragg diffraction of visible light from the 3D ordered structure. The optical measurements are complimented by theoretical calculation using a scalar-wave approximation (SWA) model.[81] The calculated spectrum in Figure 9A (red line) from a macroporous ETPTA film with close-packed 260 nm voids and 12 monolayers agree reasonably well with the experimental spectrum. This further confirms the high crystalline quality of the templated macroporous polymers.

As the hydrophobicity of the macroporous films is mostly originated from the porous top layer, while the optical diffraction is mainly contributed by the stacked multilayers, we speculate that the brief oxygen RIE process which is used to control the size of the top-layer voids will have small effect on the final optical properties of the macroporous films. Figure 9B shows the optical reflectance measurements on 11 samples created by oxygen RIE of a macroporous ETPTA film templated from 260 nm silica spheres for different durations. Although the amplitude of the zeroth-order diffraction peak located at 482 nm reduces slightly with longer etching time, the shift of the peak position is less than 1 nm for all samples. As the diffraction amplitude is sensitive to the crystalline thickness,[82] the effect of oxygen etching on the final reflectance can be significantly reduced by using thicker films.

Conclusions

In conclusion, we have developed a scalable templating technology for fabricating flexible macroporous polymer films with excellent water-repelling and optical diffractive properties. All procedures involved in the fabrication of superhydrophobic macroporous films, including doctor blade coating, oxygen plasma etching, hydrofluoric acid washing, and surface functionalization, can be made compatible with roll-to-roll processing for large-scale production of flexible self-cleaning diffractive optical devices.

Acknowledgment. This work was supported in part by the NSF CAREER Award under Grant CBET-0744879, ACS Petroleum Research Fund, California Energy Commission, and the start-up funds from the University of Florida. The authors thank Ms. Chen Dong for her assistance with the bacterial contamination tests.

(78) Weissman, J. M.; Sunkara, H. B.; Tse, A. S.; Asher, S. A. *Science* **1996**, *274*, 959–960.
(79) Pan, G. S.; Kesavamoorthy, R.; Asher, S. A. *Phys. Rev. Lett.* **1997**, *78*, 3860–3863.
(80) Kim, S. H.; Jeong, W. C.; Yang, S. M. *Chem. Mater.* **2009**, *21*, 4993–4999.
(81) Mittleman, D. M.; Bertone, J. F.; Jiang, P.; Hwang, K. S.; Colvin, V. L. *J. Chem. Phys.* **1999**, *111*, 345–354.
(82) Bertone, J. F.; Jiang, P.; Hwang, K. S.; Mittleman, D. M.; Colvin, V. L. *Phys. Rev. Lett.* **1999**, *83*, 300–303.